March 2019

Investigation of Gas Transport Phenomena in Gas Diffusion Layers of Proton Exchange Membrane Fuel Cells

Deanna Lemay Poirier
Worcester Polytechnic Institute

Laura Auerbach
Worcester Polytechnic Institute

WPI

Investigation of Gas Transport Phenomena in Gas Diffusion Layers of Proton Exchange Membrane Fuel Cells

Authors:

Laura Auerbach

Deanna Poirier

March 1, 2019

A Major Qualifying Project Report

Submitted to the faculty of
WORCESTER POLYTECHNIC INSTITUTE
In partial fulfilment of the requirements for the
Degree of Bachelor of Science

Submitted to:
Professor Kmiotek

Co-Advised by:
Caroline Bonnet (ENSIC)
François Lapicque (ENSIC)

Abstract

Proton exchange membrane fuel cells are a potential source of energy for commercial use, but efficiency is insufficient for feasible implementation. Research has been focused on improving the cell's individual components, and this report focuses on the permeability of the gas diffusion layer. Global, through-plane, and in-plane permeabilities were tested using nitrogen, hydrogen, and mixtures of the gases in ratios 1:1 and 2:1 (N_2:H_2). Two different modified cells were used to test the permeability types by manipulating gas flow direction. Darcy's Law with the Forchheimer term was used for permeability calculations. It was found that the presence of an MPL lowers GDL permeability and has a greater impact on through-plane permeability than in-plane permeability.

Keywords; PEM Fuel Cells, Transport phenomena, Gas diffusion Layers, Permeability

Acknowledgements

We would like to thank the École Nationale Supérieure des Industries Chimiques (ENSIC) and specifically the LRGP group for the use of their laboratory and facilities.

We would also like to thank our sponsors François Lapicque and Caroline Bonnet who provided us with guidance and support throughout our project. A special thank you to our mentor, and PhD student, Mainak Mukherjee for designing, overseeing, and assisting us with the experiments.

We would like to thank our advisor Stephen Kmiotek for his input throughout the project and helpful feedback on our work.

Table of Contents

Table of Figures

Table of Tables

1. Introduction

Recently, more research has been conducted on fuel cells as an alternative source of energy to fossil fuels and natural gas. Proton exchange membrane fuel cells (PEMFCs) have been one of the most promising types of fuel cells for commercial implementation, but the technology is not efficient enough to feasibly replace mainstream energy sources. A majority of the research is focused on improvement of the materials of construction and on the design of individual parts of the fuel cell, such as the gas diffusion layer (GDL) which assists in the uniform distribution of reactants to the catalyst and helps the flow of current through the cell.

In PEMFCs, the reactants, hydrogen and air (oxygen), must be able to efficiently pass through the GDL in order for the reaction to take place and produce energy. Understanding how GDL properties such as thickness, presence of a microporous layer (MPL), and hydrophobic treatment correlate to permeability of the layer is therefore important. If the permeability is too high, the diffusion rate will increase, and water will be produced as a byproduct more quickly than it can be removed. This ultimately leads to degradation of the cell. If the permeability is too low, inhibition of reactant movement throughout the cell will occur and diffusion rate will decrease. Although the presence of an MPL decreases diffusion rate, its improvement of water management makes it a critical part of the GDL. As there is a balance between permeability and optimal water management, it is important to understand the gas transport phenomena within the GDL.

Overall permeability of the GDL, or global permeability, is made up of two components: through-plane permeability and in-plane permeability. A large amount of research has been done on global and through-plane permeability of GDLs. However, more research needs to be done for in-plane permeability as no significant literature values have been reported. The objective of these experiments was to gain a better understanding of the relationship between the properties of a GDL and its permeability by assessing the global, through-plane, and in-plane permeabilities of 10 GDLs.

Permeabilities were tested using nitrogen, hydrogen, and mixtures of the gases in ratios 1:1 and 2:1 (N_2:H_2). Two different modified cells, multichannel and fundamental, were used to test the different permeability types by manipulating gas flow direction. Darcy's Law with the Forchheimer term was used for permeability calculations.

2. Background

2.1 Fundamentals of Fuel Cells

Fuel cells generate energy in the form of electricity through the application of electrochemistry. Electrochemistry is a branch of chemistry that combines electrical and chemical principles. Fuel cells utilize this process to oxidize a fuel, creating a current and heat. A basic fuel cell has three main components: an anode, a cathode, and an electrolyte. Both the anode and the cathode include a catalyst layer and a gas diffusion layer. The cathode donates electrons to the reaction while the anode absorbs electrons from the reaction. Furthermore, the anode is the region of the cell where the fuel enters, while the oxidizer enters through the cathode. The electrolyte is located between the two electrodes. Fuel cells have the potential to be a viable source of energy in today's society if the technology can be optimized to achieve higher efficiencies [1].

2.1.1 Associated Half Cell Equations

There are two main reactions that occur in a fuel cell, one at the anode and one at the cathode, as seen in Figure 1. Many fuel cells use hydrogen for the fuel entering at the anode and use air as the oxidizer at the cathode. The overall reaction [1] that is taking place within the fuel cell is

$$2H_2 + O_2 \rightarrow 2H_2O \ + \ heat \ + electricity$$

At the anode, hydrogen is oxidized, which causes it to release electrons, H^+ ions, and heat.

$$2H_2 \rightarrow 4H^+ + 4e^-$$

At the cathode, oxygen reacts with the H^+ ions from the electrolyte and the electrons from the anode reaction.

$$O_2 + 4e^- + \ 4H^+ \rightarrow 2H_2O$$

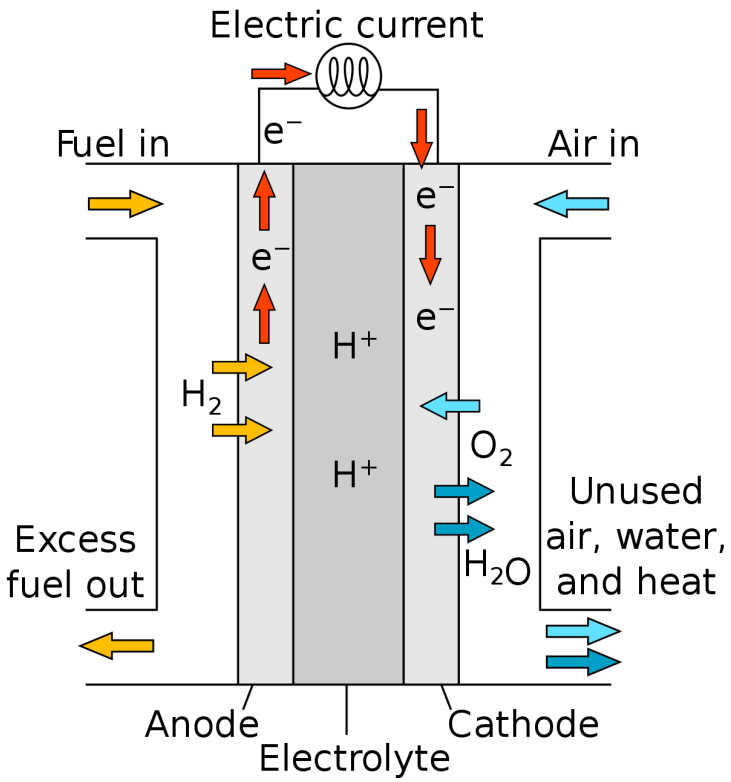

Figure 1. Basic layout of a PEMFC [2]. The anode and cathode can be seen with their respective reactions. The flow of electrons is also shown.

2.1.2 Types of Fuel Cells

There are various types of fuel cells that can be used depending on the desired application. Fuel cells are classified based on the electrolyte used as well as the temperature they operate at. Different fuels are used for different cells, but H_2 is the most common. A summary of the most common fuel cells can be seen in Table 1 [1].

Table 1. Common fuel cells and their properties.

Fuel Cell Type	Mobile Ion	Operating Temperature (°C)	Fuel	Applications and Notes
Alkaline (AFC)	OH^-	50-200	Pure H_2	Space vehicles, e.g., Apollo, Shuttle
Proton exchange membrane (PEMFC)	H^+	30-100+	Pure H_2	Vehicles and mobile applications, and for low power CHP systems
Direct Methanol (DMFC)	H^+	20-90	Methanol	Portable electronic systems of low power, running for long times
Phosphoric Acid (PAFC)	H^+	~220	H_2, (low S, low CO, tolerant to CO_2)	Large numbers of 200-kW CHP systems in use
Molten Carbonate (MCFC)	CO_3^{2-}	~650	H_2, various hydrocarbon fuels (no S)	Medium- to large-scale CHP systems, up to MW capacity
Solid Oxide (SOFC)	O^{2-}	500-1000	Impure H_2, variety of hydrocarbon fuels	All sizes of CHP systems, 2 kW to multi MW

2.2 PEMFCs

Proton exchange membrane fuel cells, also known as polymer electrolyte membrane fuel cells, are acid fuel cells used in various applications such as the automotive industry and for portable electronics [3-5]. They typically use pure H_2 as a fuel, which does not produce emissions [3, 4, 6]. Platinum supported on carbon is typically used as the catalyst [7].

One advantage of PEMFCs is their quick start up, which can be achieved because the fuel cell can operate at ambient temperature. Between ambient temperature and 60°C, the cell is able to keep itself humidified. This humidification is essential for the continued efficiency of PEMFCs. However, the performance of the fuel cell increases as temperature increases. At these higher temperatures, it is necessary to humidify the equipment externally by passing the inlet gases through a humidifier. If the components within the fuel cell become dry, the overall cell performance will decrease, and the cell may begin to degrade [8].

2.2.1 Parts of a PEMFC

PEMFCs are made up of bipolar plates and a membrane electrode assembly (MEA), which contains a proton exchange membrane, two catalyst layers, and two gas diffusion layers.

Bipolar Plates

Bipolar plates can be used to connect various MEAs, as seen in Figure 2 [1]. In a system with a single MEA, the bipolar plates act as bookends to the fuel cell setup. The bipolar plates aid the flow of gas throughout the fuel cell. They also help with electron conduction and heat removal [9].

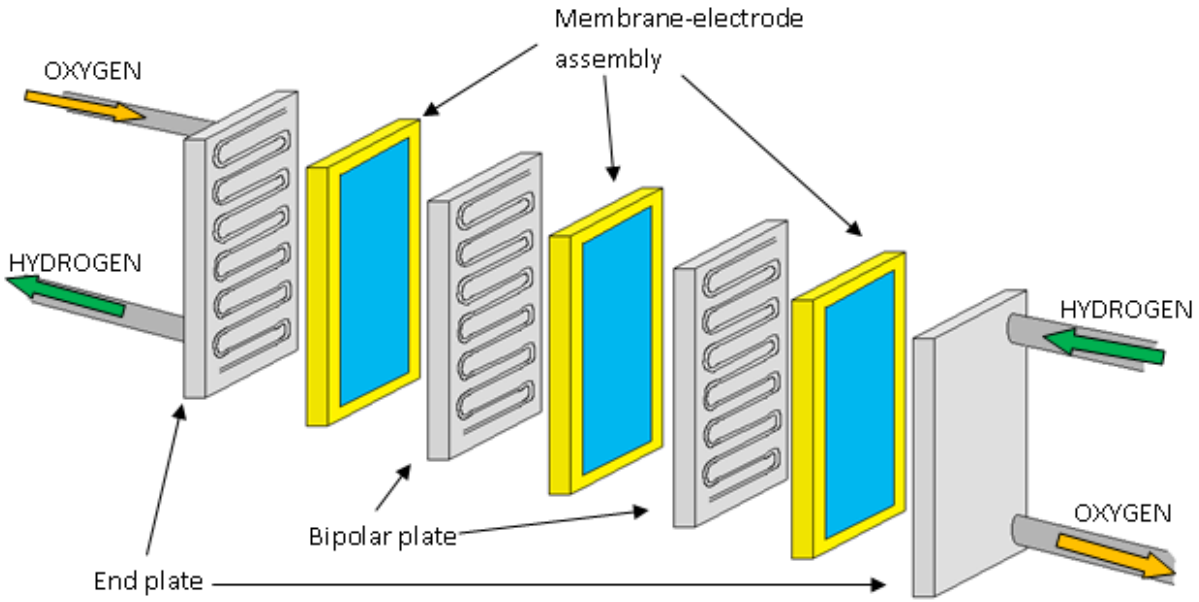

Figure 2. Multiple MEAs connected in series using bipolar plates [10].

Membrane Electrode Assembly (MEA)

The proton exchange membrane, catalyst layers, and GDL make up the membrane electrode assembly [6]. PEMFCs are one of the few types of fuel cells that use a solid electrolyte source, rather than a liquid source. This solid proton exchange membrane can be considered a gel and allows for protons to pass from the anode to the cathode [9]. Since it is solid, it enables the parts of the fuel cell to be layered to create a thin set up, as seen in Figure 3 [1]. The proton exchange membrane is lined with catalyst on both sides, which is generally made of platinum dispersed on carbon black. The catalyst layers are then covered with the gas diffusion layer (GDL), which is used for electron conduction, a path for the reactants to uniformly reach the catalyst, and for water removal [6, 9].

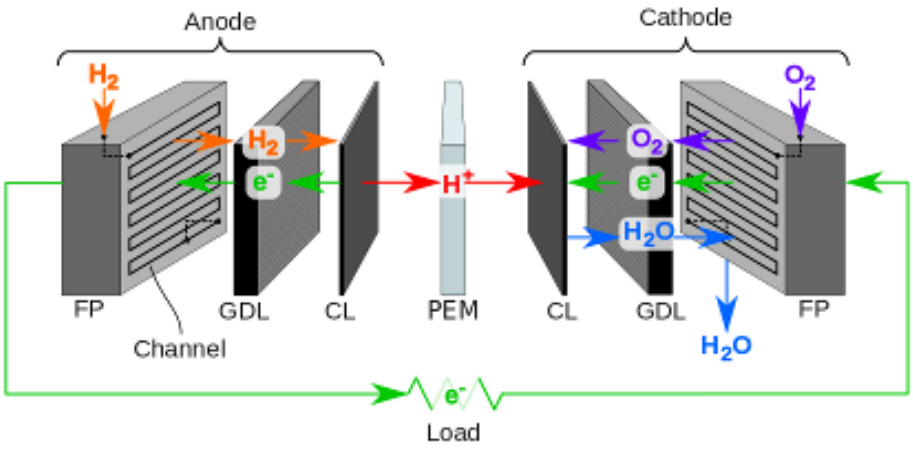

Figure 3. Breakdown of the layers within a PEMFC. The PEM is lined with a catalyst layer on both sides, which are covered with GDLs [11].

2.2.2 Limitations

One of the major challenges with fuel cells is improving their efficiency. Within a PEMFC, there are three main factors that lead to energy loss: activation losses, ohmic losses, and gas transport losses. Activation losses at the electrodes are associated with cell start up, ohmic losses within the membrane are proportional to the length of the cell, and gas transport losses are mainly caused by the deterioration of the GDL. Each of these losses is most easily seen at a certain range of voltage and current density. For example, activation losses are seen when the fuel cell has a high voltage and low current density because these values are inversely proportional. However, it is important to note that all three losses can occur at any time. These losses can be represented by a polarization curve as seen in Figure 4.

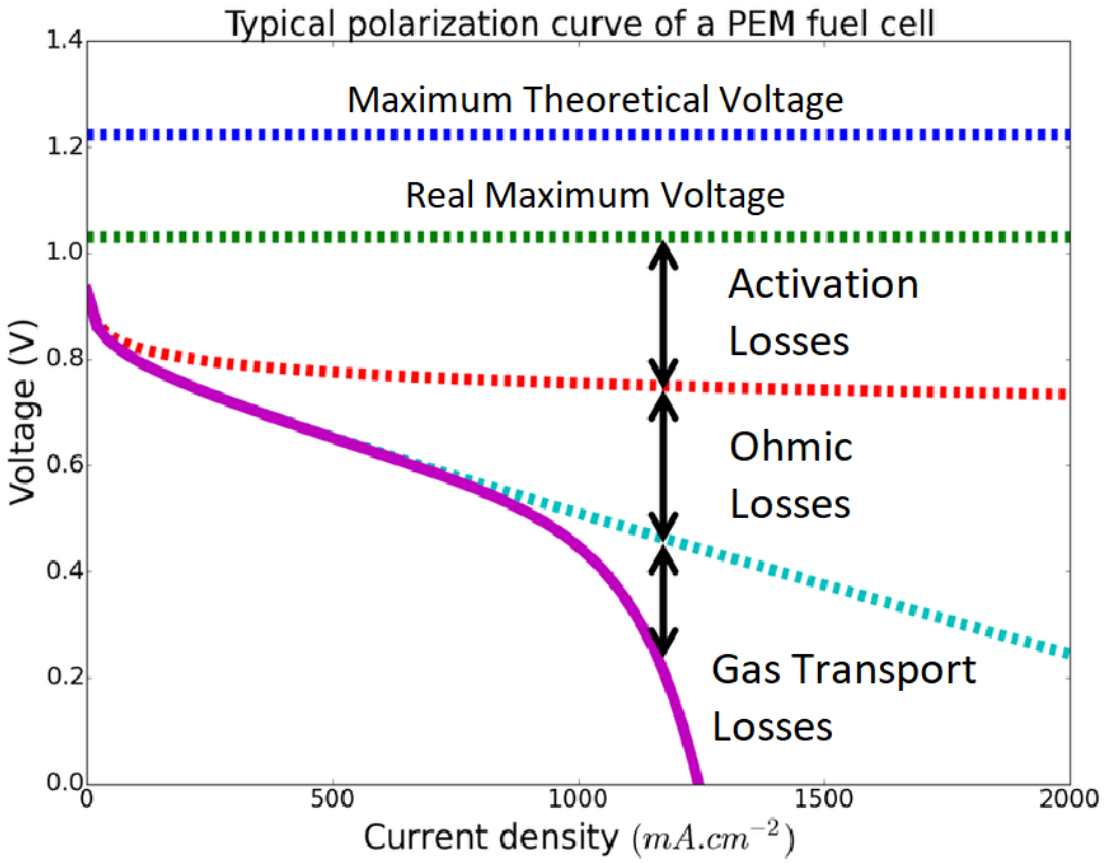

Figure 4. Polarization curve of a PEMFC. The three main causes of voltage losses are shown [12].

2.3 Gas Diffusion Layer

The gas diffusion layer (GDL) typically consists of carbon fibers and is the flexible part of the MEA that supports the structure while holding the catalyst layer. Acting as a connection between the bipolar plates and the electrode, the GDL helps current to flow through the cell [13]. The GDL allows for water and gas to flow countercurrent by evenly distributing the gas from the flow channels of the bipolar plates to the catalyst while simultaneously removing water and heat from the catalyst into the flow channels [6].

2.3.1 Composition of a GDL

Currently, the most common type of GDL is comprised of two main components: the macroporous substrate (MPS), also known as the gas diffusion backing (GDB), and the microporous layer (MPL) [6]. Prior to the inclusion of the MPL, GDLs commonly consisted of only the MPS which was found to have poor water management, resulting in accelerated degradation of the cell and ultimately reduced overall efficiency [14]. For this reason, the MPL

was introduced to improve the removal of water from the cathode of the cell as it is produced via chemical reaction. The two different layers of the GDL can be seen below in Figure 5.

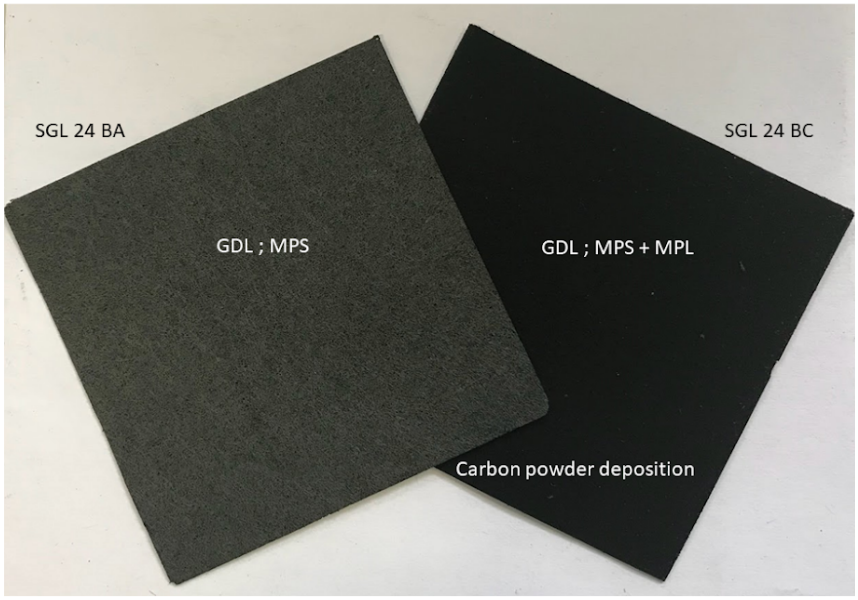

Figure 5. The MPS and MPL layers of the GDL.

In the fuel cell, the GDL is oriented so that the MPL is in contact with the catalyst layer to maximize the layer's ability to circulate and remove water from the cell. The MPS is positioned next to the gas flow field to facilitate the permeation of gas through the fuel cell and to the membrane. Figure 6 below shows the orientation of these layers within the GDL.

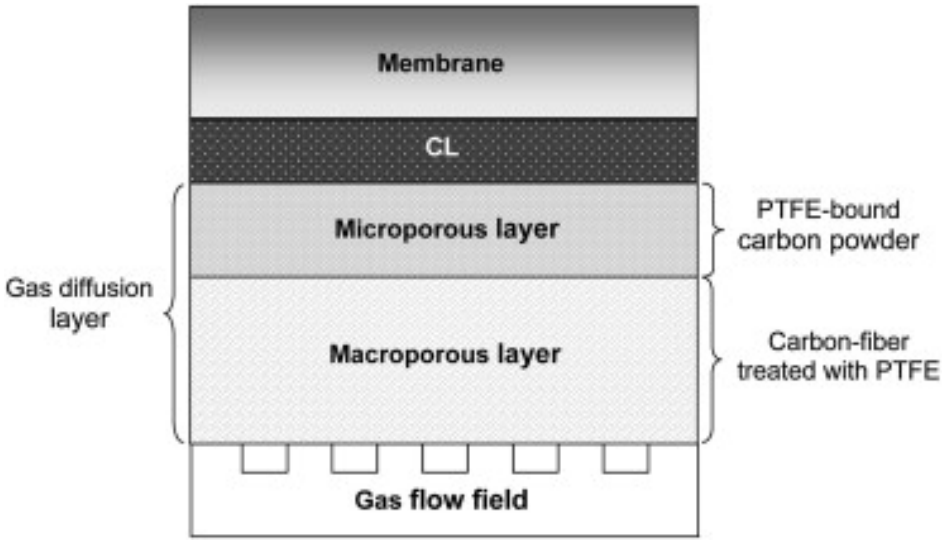

Figure 6. GDL construction and orientation within a fuel cell [15].

Macroporous Substrate (MPS)

The macroporous substrate (MPS) is used to collect current from the fuel cell and connects the flow field to the MPL. The MPS comes in two forms: carbon paper and carbon cloth. Carbon paper MPSs are typically thinner than carbon cloth. The paper MPSs also have increased porosity since the fibers are more spaced out. The random arrangement of the fibers leads to the anisotropy of the MPS. Carbon paper is more brittle than carbon cloth, so more care is needed when using this type of MPS. Carbon paper is generally less compressible than carbon cloth [16]. Often this layer is treated with polytetrafluoroethylene (PTFE) to assist with water management. PTFE is a hydrophobic synthetic resin able to withstand high temperatures and is nearly chemically inert [17]. The MPS has a pore size of 1-150 μm [3].

Microporous Layer (MPL)

In order to improve the performance of the fuel cell, the MPL was added to the GDL in order to increase the functionality and durability of the layer. The MPL is composed of ink containing suspended carbon particles mixed with a hydrophobic binder (often carbon black, PTFE, or Teflon®) and is deposited onto the MPS [18]. The MPL has a pore size of 2-200 nm, which is largely affected by the amount of PTFE and carbon in the layer [3]. After the MPL is deposited onto the MPS, the GDL undergoes thermal annealing, which increases the hydrophobicity of the GDL. During this process, some of the ink particles are able to embed into the carbon fibers of the MPS, thus creating a "penetration zone" when the GDL is compressed during assembly and cell mounting [6]. Due to the MPL particles being at least an order of magnitude smaller than the MPS particles, and due to the operating conditions (T, P) of the process, the addition of the MPL leads to formation of an intermediate layer between the MPL and the MPS.

2.4 Gas Transport in Gas Diffusion Layers

The gas diffusion layer serves many functions within the fuel cell. An important purpose of the GDL is to help the reactant gases pass to the catalyst layer of the cell. The transport of gases within the GDL is important to understand in order to be able to optimize the GDL.

2.4.1 Molecular Diffusion and Convection

Two types of transport are prevalent in the cell: convection and diffusion. Because both types are occurring simultaneously, they are often referred to as convective-diffusive transport. Convective transport is seen in fuel cells as the reactants are transported across channels within the fuel cell. Diffusion is seen when these reactants pass through the GDL to the catalyst layer and membrane electrode assembly [3]. Improved mass transfer rates can lead to a reduction in the required amount of catalyst, as well as an increase in the amount of power produced [19].

2.5 Permeability in Gas Diffusion Layers

In order to understand convective-diffusive transport, it is also important to study the permeability of the GDL [3, 4]. The permeability of this layer corresponds to its porosity, which is represented as a percentage. A higher porosity indicates there is more space within the layer for gas to flow through, thereby increasing permeability.

While some research has been done on GDL permeability, most of these studies used a GDL that was coated with an MPL. Therefore, less is known about the permeability of just the MPS. Additionally, most of these studies focused on global and through-plane permeability, thus there is not much data on in-plane permeability [19]. Global permeability refers to the overall permeability of the GDL, including both through-plane and in-plane.

2.5.1 In-Plane and Through-Plane Permeability

In-plane permeability measures the flow of particles that move radially or laterally through the GDL before passing through, as seen by paths 1 and 2 in Figure 7. Although in-plane permeability through the GDL is an important factor in the performance of a fuel cell, little research has been done to understand the phenomena. This is due to the difficulty associated with taking accurate in-plane measurements [20].

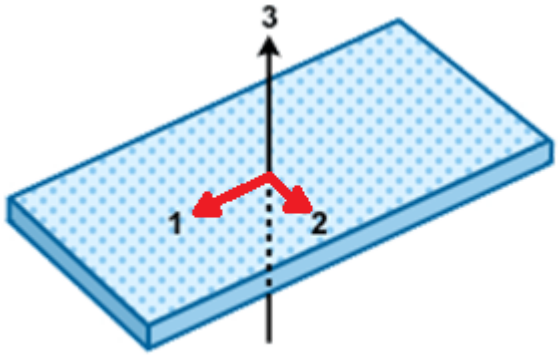

Figure 7. In-plane permeability through a medium. The flow path is shown by arrows 1 and 2 [21].

Through-plane permeability measures the flow of particles directly through the GDL, as seen by path 3 in the same figure. Through-plane transport generally occurs through diffusion, but it can also happen through convection.

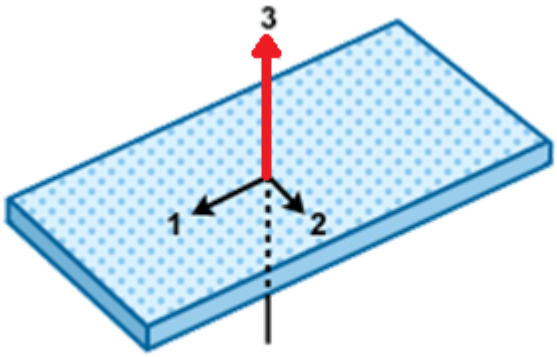

Figure 8. Through-plane permeability through a medium. The flow path is shown by arrow 3 [21].

2.5.2 Viscous and Inertial Permeability

Permeability can be split into two categories: viscous and inertial. The Navier-Stokes equation can be used to describe viscous flow of a fluid [22]. In the case of low velocities, Stokes flow can be assumed, and Darcy's law is used to describe the fluid flow through pores.

$$\frac{\Delta P}{L} = \frac{\eta v}{K_v}$$

Where ΔP: change in pressure drop (Pa)
L: length over which the pressure drop is occurring (m)
η: viscosity (Pa·s)
v: velocity ($m \cdot s^{-1}$)
K_v: viscous permeability (m^2)

In fuel cells, Darcy's Law has been used to predict the pressure drop (ΔP) across the GDL, both with and without an MPL. Pant et al. states that Darcy's Law is often not a good model due to the presence of inertial forces in the cell in addition to the viscous forces [3]. The Forchheimer term can be added to Darcy's Law in order to account for these forces [3, 23].

$$\frac{\Delta P}{L} = \frac{\eta v}{K_v} + \frac{\rho v^2}{K_i}$$

Where ρ: density ($kg \cdot m^{-3}$)
K_i: inertial permeability (m)

In order to fully understand the permeability of a material, it is important to consider both the viscous and inertial forces. However, there is little understanding of the inertial permeability in GDLs.

2.6 Impact of GDL Permeability on Fuel Cell Performance

Gaining a deeper understanding of the mass transport phenomena at work in the GDL is important to improving the efficiency of the fuel cell. Because the GDL is used to transport the reactants to the catalyst layer, it is important for effective mass transfer to be taking place. A permeability that is too high or low will lead to the cell not performing at peak efficiency.

The permeability can become too high when the GDL begins to wear. If the permeability is too high, there is increased contact resistance between the GDL and the electrodes. As a result, reactants may be consumed more quickly than new reactants are being brought to the catalyst layer. In this case, the efficiency is not at a maximum, meaning less current is being produced than is possible. This increased diffusion rate also means that the gas distribution may be less even, and water may be removed less effectively. Excess water in the cell leads to degradation, and also acts as a diffusion inhibitor. This is why proper performance of the MPL is very important [14].

Water build up in the cell is one of the biggest diffusion inhibitors, but permeability can also be low if a GDL is thick or has a high PTFE content. Presence of an MPL also decreases permeability, but its effective water management makes it an effective addition to the GDL. When permeability decreases, fewer reactants will diffuse to the catalyst layer resulting in a lower current output [23, 24].

2.6.1 Optimization of the GDL

The three main variables that contribute to GDL performance are:

1) Treating with MPS with PTFE
2) The inclusion of an MPL
3) The overall thickness of the GDL

These variables are related to the permeability of the GDL in various ways. Treating the MPS with PTFE increases its hydrophobic properties, improving the GDLs water management by helping it to repel water to avoid flooding. The improved water management allows the cell to distribute water properly, ensuring that the cell does not dry out. This leads to a decrease in mass transfer losses and contributes to an overall increased performance of the cell. Adding too much PTFE can block pores and limit diffusion, thus a content between 10-20% is ideal [4].

The inclusion of the MPL results in a hydrophobic surface which facilitates the movement of water within the cell, keeping the cell correctly humidified while removing excess water that would degrade the cell. Without this layer, water buildup can lead to flooding of the cell. In cells that contain an MPL, ohmic losses have been found to decrease. The addition of the MPL leads to a decrease in permeability due to its small pore size. Under certain operating conditions and at high current densities, it can also cause flooding on the anode side of the MEA, which leads to

increased mass transfer losses. However, the advantages generally outweigh any negatives associated with an MPL [25].

Thinner GDLs have lower ohmic losses. The addition of PTFE only causes minor changes in GDL thickness and porosity, while the addition of an MPL causes the overall thickness to notably increase. However, the advantages that come from the inclusion of the MPL generally outweigh any negative effects caused by increasing thickness. The anisotropy of the GDL often has more effect on permeability than thickness. Overall, if possible, it is best to use a thin, PTFE coated GDL that contains an MPL [18].

The compression of the GDL also leads to changes in permeability. Ihonen reports that increasing cell compression leads to reduced in-plane permeability of the GDL, which is the same trend seen for through-plane permeability under compression [26].

3. Methodology

For this study, both coated (MPS with MPL) and non-coated (MPS only) carbon paper GDLs of different thicknesses were used in order to assess the impact of different characteristics on permeability. The objective of these ex-situ experiments was to assess the permeability of 10 GDLs using cells that have been modified from normal functioning fuel cells. A multichannel cell was used to test global permeability and a fundamental cell was used to test through-plane and in-plane permeability.

3.1 Selection of GDLs and Gas Configuration

The experiments were conducted using the following 10 GDLs: 10 BC, 24 AA, 24 BA, 24 BC, 28 AA, 28 BC, 30 BC, 34 BA, 34 BC, and 38 BC. This report will focus on 34 BA, 34 BC, 24 BA, and 24 BC due to limitations on report length and to concisely convey the main trends observed.

Table 2. Properties of GDLs [27, 28].

GDL Type	PTFE Content of MPS	MPL	Basic Weight ($g \cdot m^{-2}$)	Thickness (μm)	Porosity
24 AA	0%	No	51	190	-
24 BA	5%	No	54	190	84%
24 BC	5%	Yes	100	235	76%
28 AA	0%	No	55	190	82%
28 BC	5%	Yes	105	235	80%
34 BA	5%	No	86	280	83%
34 BC	5%	Yes	140	315	75%
10 BC	5%	Yes	135	420	82%
30 BC	5%	Yes	-	340	-
38 BC	5%	Yes	125	325	80%

Sigracet (SGL) GDLs were used for all experiments in this report. Sigracet has a simple naming system for their GDLs.

1) The GDLs all contains a number paired with two letters
2) GDLs named AA are plain carbon fiber and do not contain an MPL or any PTFE
3) GDLs named BA do not contain an MPL but do contain 5% PTFE
4) GDLs named BC contain an MPL and 5% PTFE

The cells were tested using pure nitrogen and pure hydrogen in order to determine the difference in permeability of the two gases and understand how molecular size and viscosity of the fuel cell reactants (air and hydrogen) impacts permeability of the GDL. Mixtures of hydrogen and nitrogen were also tested in four ratios to gain a deeper understanding of the effect of different conditions during actual operation. The ratios were 1:1, 2:1, 2.5:1.2, and 3:1.2 (N_2:H_2). Only ratios 1:1 and 2:1 will be discussed for simplicity.

Pure nitrogen was used to represent air during experimentation as nitrogen is more chemically inert than air. This avoided the reaction between oxygen in air and hydrogen, which would produce water. The use of nitrogen in place of air was justified because air is mostly nitrogen, and because the molecular weight, size, and viscosity of air and nitrogen are similar.

3.2 Multichannel Cell and Fundamental Cell Design

3.2.1 Multichannel Cell

There are various types of bipolar plates, the most common being square-ribbed, single-channel, and multi-channel. These plates, seen in Figure 9, each allow for a different flow of the gas through the fuel cell.

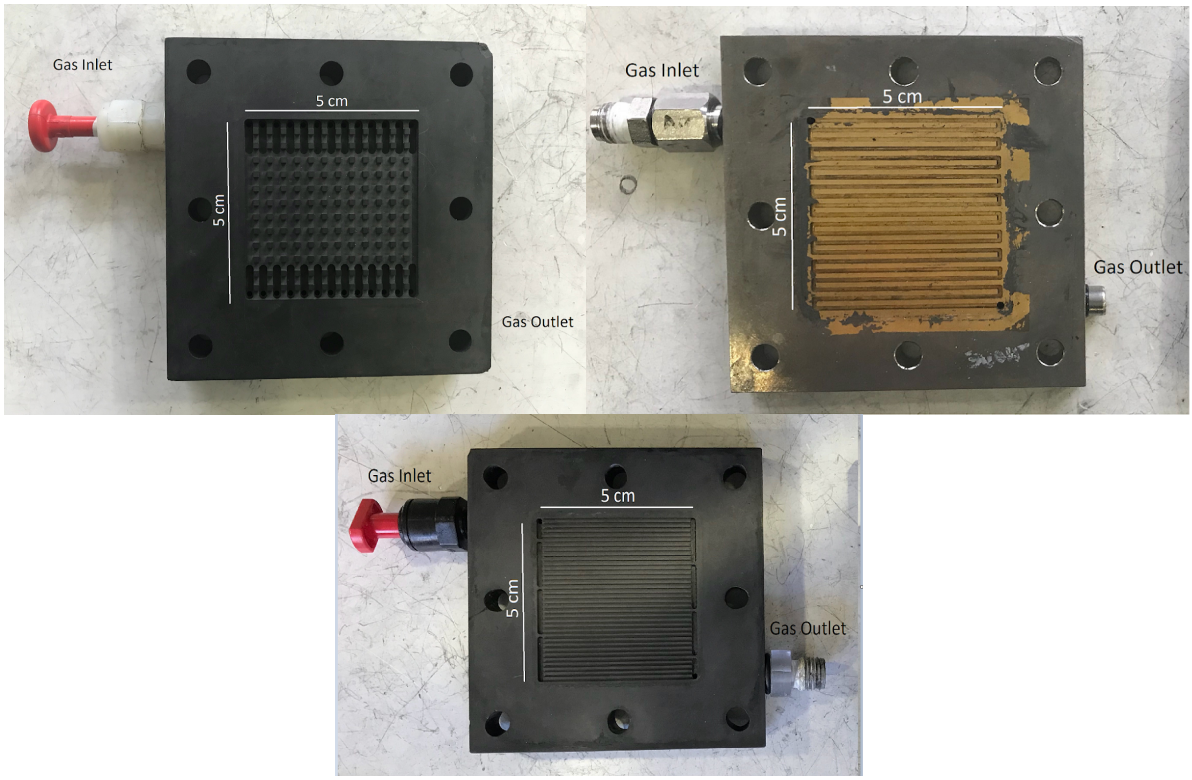

Figure 9. A square-ribbed, single-channel, and multi-channel bipolar plate.

Each of these bipolar plates have the same overall dimensions, 5 cm x 5 cm. However, each has different specific dimensions, as seen in Table 3. It is important to note that the multichannel cell has two different sized ribs.

Table 3. Dimensions of bipolar plates.

Type	Rib Length (10^{-2} m)	Rib Width (10^{-3} m)	Number of Ribs	Effective Surface Area* (10^{-3} m^2)
Square-Rib	0.166	1.66	144	2.18
Single-channel	4.9	1.3	20	1.31
Multi-channel	4.77	0.6	28	1.61
	4.88	0.6	6	

*The surface area of the bipolar plate that does not come in contact with the GDL and allows for the flow of gas throughout the cell

In order to study global permeability, a multichannel cell was used, as seen in Figure 10.

Figure 10. Assembled multichannel cell.

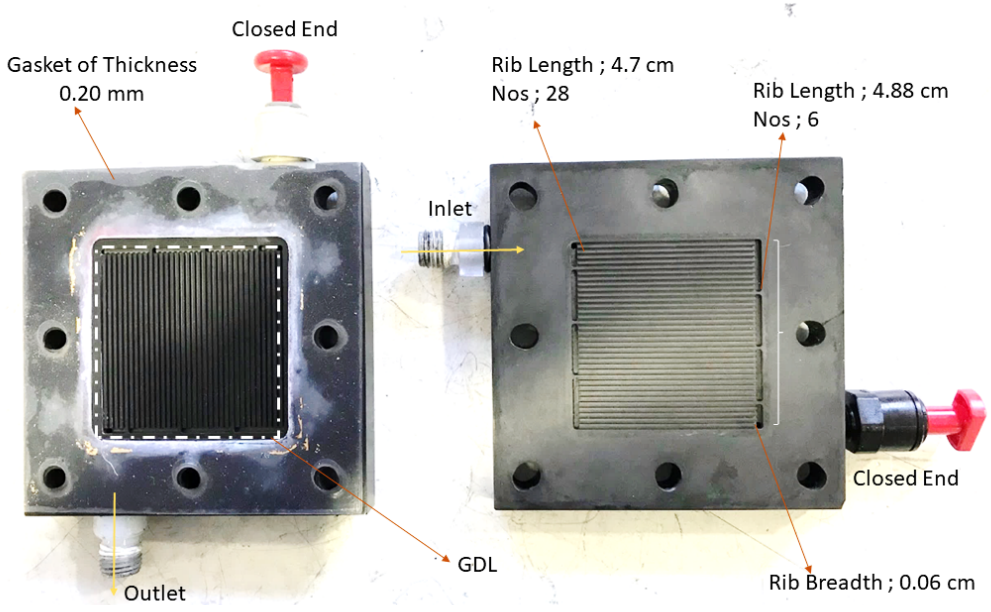

Figure 11. Disassembled multichannel cell. The cathode bipolar plate (left) and anode bipolar plate (right) can be seen.

The cell is made up of two bipolar plates which each have an inlet and outlet for gas to flow through. As can be seen in Figure 11, the top cell is oriented so that the channels for gas flow are vertical and the gas inlet and outlet are located on the top and bottom of the plate. The bottom plate has the flow channels oriented horizontally and the inlet and outlet are located on the left

and right of the plate. On each plate, one of the outlets was plugged with a red stopper so that when the multichannel cell was assembled, the gas is forced to flow in the bottom plate's inlet, through the gas flow channels and across the GDL to the other plate, through the top plate's gas flow channels, and exits via the top plate's outlet. This setup ensures that the gas must flow through the GDL in order to leave the system, thereby allowing for accurate permeability calculations to be performed.

When conducting tests, a GDL cut to 5.2 cm x 5.2 cm was placed between the plates to cover the gas flow channels. Prior to testing, the thickness of the GDL was recorded and compared to literature values. When using a GDL with an MPL, the MPS side faced the inlet (bottom) bipolar plate and the MPL side faces the outlet (top) bipolar plate. In a real cell, the MPL faces the catalyst side to help facilitate the movement of water through the cell. Although no catalyst was used for these experiments, the correct orientation of the GDL was used to simulate a real fuel cell.

For each of the GDLs, the cell was loaded and then tightened to 1.5 N·m and then 3.5 N·m. Incremental tightening allowed for even compression of the GDL to avoid damage. Flow rates between 50-500 $NmL \cdot min^{-1}$ were tested in increments of 50 $NmL \cdot min^{-1}$.

3.2.2 Fundamental Cell

In order to assess the two components of global permeability (through-plane permeability and in-plane permeability) for various MPLs, ENSIC's LRGP group developed the fundamental cell, as seen in Figure 12. This cell has one inlet and two outlets for gas. The channel for gas flow through the cell is 5 mm wide. For each run, only one outlet is used and the other is shut so no gas can pass through. Depending on which outlet is used, either in-plane or through-plane permeability can be studied.

For each of the GDLs, the cell was loaded and then tightened to 1.0 N·m. Flow rates between 10-150 $NmL \cdot min^{-1}$ were tested in increments of 10 $NmL \cdot min^{-1}$.

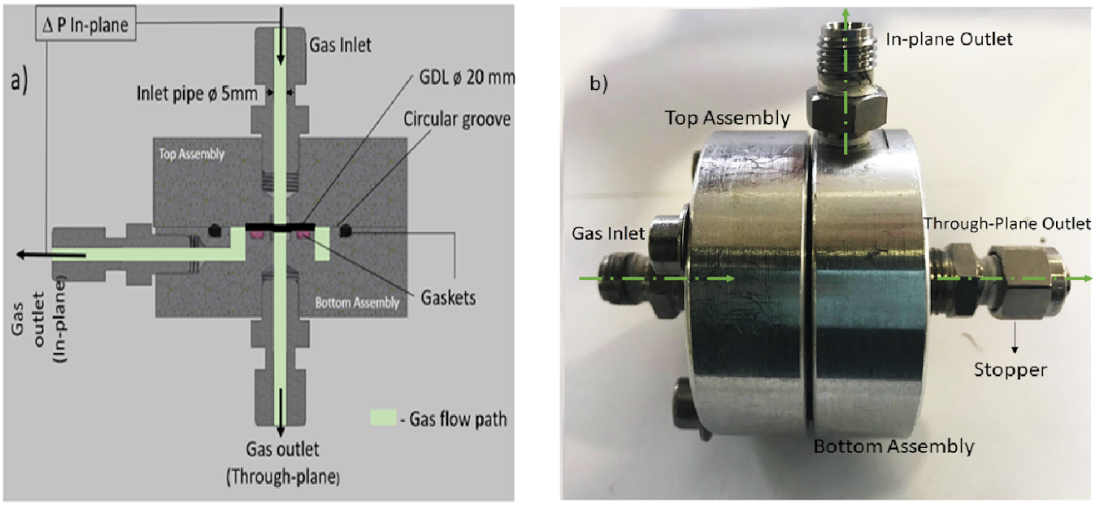

Figure 12. Assembled fundamental cell.

Through-Plane Permeability

When the through-plane outlet is open and the in-plane outlet is sealed, the gas is forced to travel through-plane. For this configuration, a 20 mm diameter circular sample of GDL was cut and placed within the fundamental cell. However, the channel for gas flow through the cell is 5 mm wide.

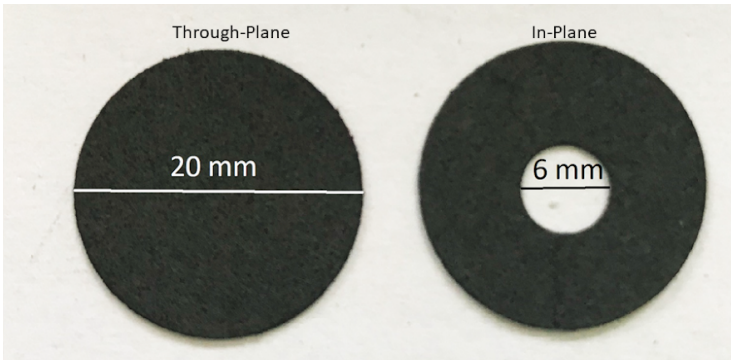

Figure 13. Prepared GDL samples for the fundamental cell. The difference between through-plane (left) and in-plane (right) GDLs can be seen.

In-Plane Permeability

When the in-plane outlet is open and through-plane outlet is sealed, the gas is forced to travel radially through the GDL, representing in-plane permeability. For this configuration, a 20 mm diameter sample of circular sample of GDL was cut and a 6 mm hole was cut in the center of the sample to allow for radial permeation through the GDL.

3.3 Experimental Setup

The general setup used can be seen in Figure 14.

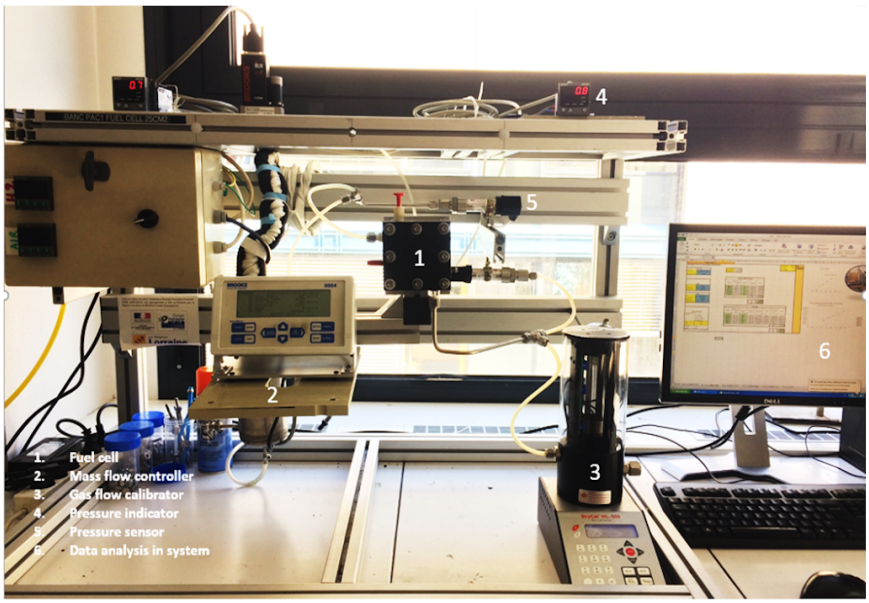

Figure 14. Overall equipment setup. The multichannel cell is shown here and can be replaced with the fundamental cell.

The nitrogen and hydrogen gases are fed from gas lines located on the adjacent wall and are each connected to a Brooks 0254 low voltage mass flow controller in order to regulate flow rates entering the cell. A gas calibrator is connected to the cell's outlet gas stream in order to measure the flow rate of gas exiting the cell. To get an accurate outlet flow rate, the average of 3 measurements was recorded. The average of the inlet and outlet flow rates was used for calculations. The two measurements were used to ensure that there were no leaks in the system: a large difference was indicative of a loose connection. A differential pressure indicator was used to measure the difference in pressure between the inlet and outlet of the cell. Operating temperature was recorded for each trial and was always between 20-25°C.

3.4 Data Analysis

Data calculations for all experiments were performed using an Excel spreadsheet which was modified for the type of testing being performed. Overall, three master spreadsheets were developed, the major difference being the effective surface area based on what type of cell was used for the experiment. Each spreadsheet used the pressure drop across the GDL and the average gas velocity for each trial to calculate viscous and inertial permeability using Darcy's Law and the Forchheimer term as a model to fit the data. The spreadsheets factored in the viscosity and density of each gas or mixture at operating conditions in order to calculate the viscous and inertial permeabilities, respectively. For each master spreadsheet the only data that

needed to be inputted for each calculation were the measured thickness of the GDL being tested, the raw data collected, and the temperature at which each experiment was conducted since viscosity and density depend on temperature.

Gas Viscosity

In order to calculate the viscosity for each gas mixture [28], the following equation was used:

$$\eta_{mix} = \frac{\sum_{i=1}^{N} y_i * \eta_i * \sqrt{M_i}}{\sum_{i=1}^{N} y_i * \sqrt{M_i}}$$

where η_{mix}: viscosity of the gas mixture (Pa·s)
y_i: mole fraction of i^{th} gas component
η_i: viscosity of the i^{th} gas component at working temperature and atmospheric pressure using Sutherland's law (Pa·s)
M_i: molecular weight of the i^{th} gas component ($g \cdot mol^{-1}$)
N: number of components in the gas mixture

Table 4. Viscosity of gases.

Gases	N_2	H_2	N_2:H_2 (1:1)	N_2:H_2 (2:1)
Calculated Viscosity (10^{-5} Pa·s)	1.744	0.8741	1.641	1.723

The viscosities in Table 4 were calculated at 20℃. Although operating temperature ranged between 20-25℃, all permeability calculations were done at 20℃ in order standardize the comparison of the values.

Pressure Gradient

For each trial, the pressure drop was recorded. However, these data had to be corrected to measure only the pressure drop that was caused by the GDL since there would be a pressure drop even if the cell was empty. Therefore, the pressure drop was recorded for an empty cell, and for each trial the actual pressure gradient across the GDL was calculated by subtracting the pressure drop across the empty cell from the measured pressure drop during experimentation.

Average Gas Velocity

In order to calculate average gas velocity, the following equation was used:

$$v_{avg} = \frac{Q}{A}$$

Where v_{avg}: average velocity of the gas ($m \cdot s^{-1}$)
Q: average flow rate of the gas measured during experimentation ($m^3 \cdot s^{-1}$)
A: effective surface area; 1.61×10^{-3} for multichannel, 1.963×10^{-5} for through-plane in the fundamental cell (m^2)

Once the average velocity and pressure gradient values were determined, Darcy's Law with the Forchheimer correction was used to model and solve for viscous and inertial permeability. Figure 15 in section 4 shows how the data would be modeled if only Darcy's Law was used, and therefore emphasizes the need for the Forchheimer term.

3.4.1 Global Permeability

For multichannel tests, the effective surface area was found to be 1.61×10^{-3} m^2. This was calculated by determining the surface area of the GDL that would come into contact with the gas passing through the flow channels. This value was obtained by subtracting the surface area of the ribs, which do not come into contact with the gas, from the total surface area of the cell that contains channels.

3.4.2 Through-Plane Permeability

For through-plane tests, the effective surface area is 1.963×10^{-5} m^2 which is equivalent to the cross-sectional area of the fundamental cell's gas outlet which had a diameter of 5 mm. This value is used because the area of the outlet is the only section of the GDL that the gas can flow through in order to exit the cell.

3.4.3 In-Plane Permeability

For in-plane tests, the area of the center hole cut out of all GDL samples must be subtracted out when calculating effective surface area. To determine the effective surface area, the GDL was assumed to be a cylindrical disk and gas could only flow radially out the sides of this cylinder to exit the fundamental cell. As such, the effective surface area is a function of the radius and was calculated to be 2.86×10^{-4} m^2.

Following these assumptions, the previous average velocity equation can be modified to:

$$v_{avg} = \frac{Q}{2\pi L(R-r)}(\ln\frac{R}{r})$$

Where R: radius of the GDL sample (m)
r: radius of the center hole in the GDL (m)
L: thickness of the GDL sample (m)

4. Results and Discussion

Prior to calculating permeability for each GDL using the Excel spreadsheets, the pressure gradient was graphed vs the average velocity for each gas configuration. This was done in order to understand the effect of different GDL characteristics on the gas transport phenomena occurring within the cell. These data were then used in conjunction with the Darcy/Forchheimer equation in order to obtain permeability values. Figure 15 shows an example of the data being modeled using only Darcy's Law. The Forchheimer correction allows for the data to be more accurately modeled because it includes inertial permeability in addition to the viscous permeability. This correction is needed at high velocities, and therefore is more relevant to calculations done in the multichannel cell, which was operated at higher velocities than the fundamental cell. While the Forchheimer term was kept for all calculations, it often became 0 when the Excel Solver function was used in through-plane and in-plane calculations.

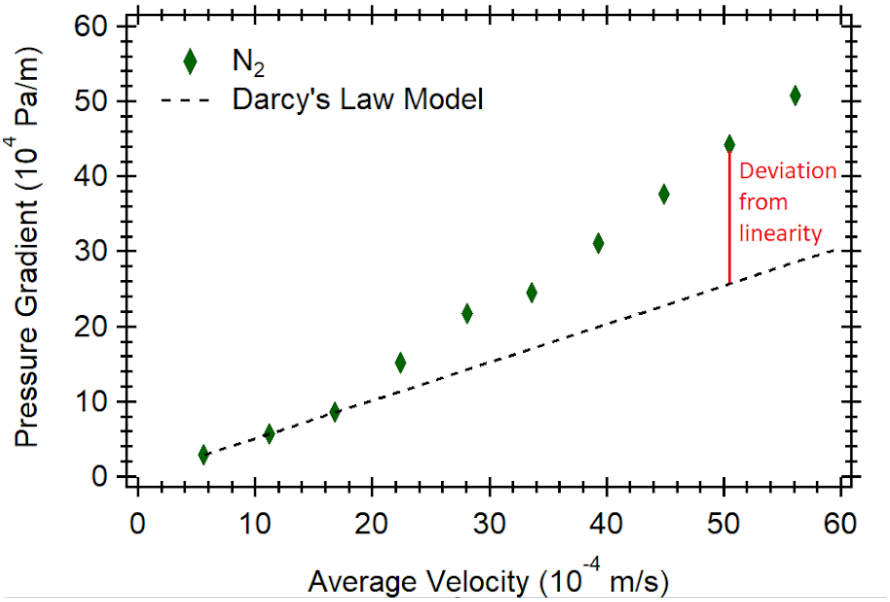

Figure 15. Inaccuracy of using Darcy's Law to model data. The pressure gradient vs average velocity for 34 BA multichannel test is shown with the Darcy's Law fit. Flow rate: 50-500 NmL·min^{-1}. Effective surface area: 1.61 × 10^{-3} m^2.

4.1 Multichannel Cell - Global Permeability

Figure 16 shows the pressure gradient vs average velocity graphs for 24 BA, 24 BC, 34 BA, and 34 BC. It can be seen that for all gas configurations, average velocity and pressure differential correlated and that as the average velocity of the gas increased, the pressure gradient across the GDL also increased. It was observed that as the average velocity increased, the greatest pressure gradient across the multichannel cell was for pure nitrogen, followed by 2:1 (N_2:H_2), 1:1 (N_2:H_2), and pure hydrogen. The large pressure differential for nitrogen is due to nitrogen's higher

viscosity of 1.74 x 10^{-5} Pa·s while hydrogen's viscosity is only 8.74 x 10^{-6} Pa·s. A lower viscosity means the gas flows more easily and therefore would decrease pressure buildup on one side of the cell. Also, nitrogen is a larger molecule with a kinetic diameter of 364 pm as compared to hydrogen's smaller kinetic diameter of 269 pm. Furthermore, nitrogen has a molecular weight of 28 while hydrogen has a molecular weight of only 2. Both of these properties fundamentally explain why nitrogen has a higher viscosity and therefore support the results obtained.

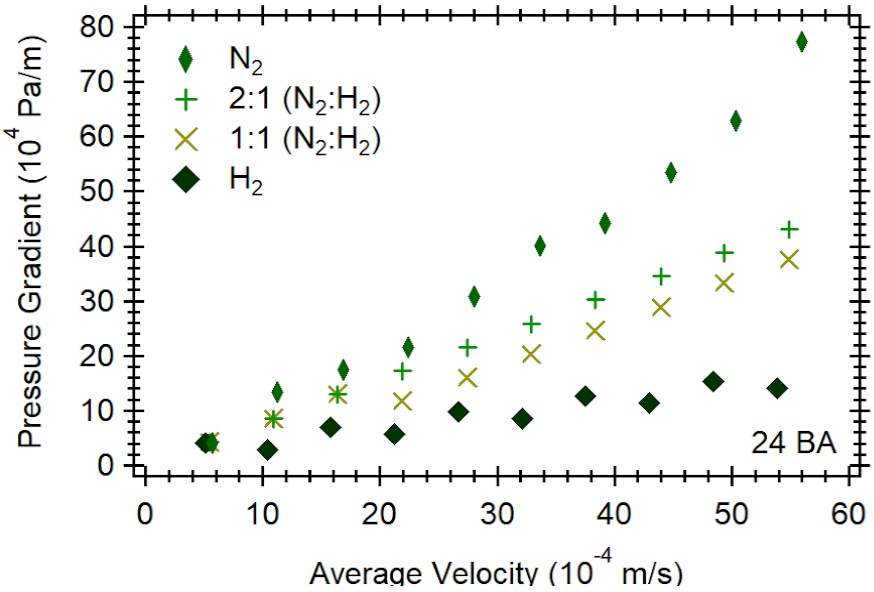

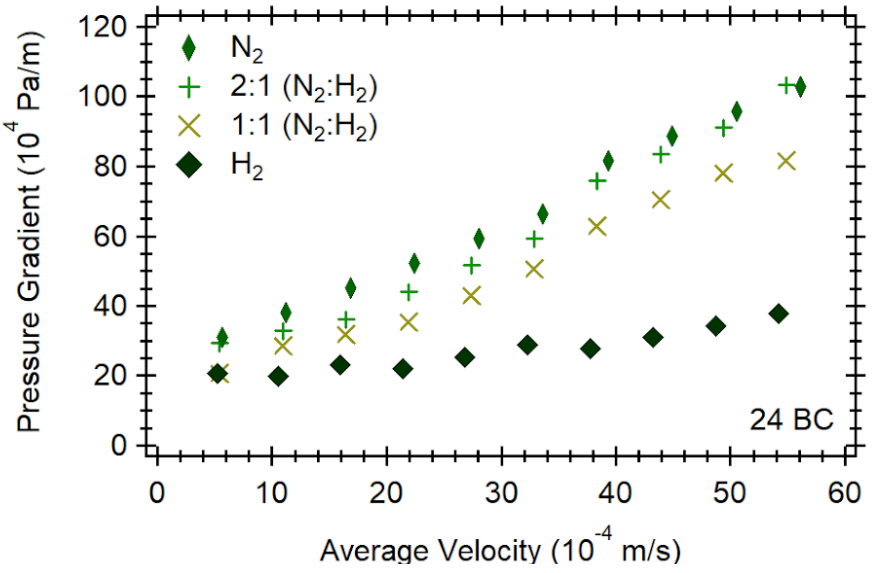

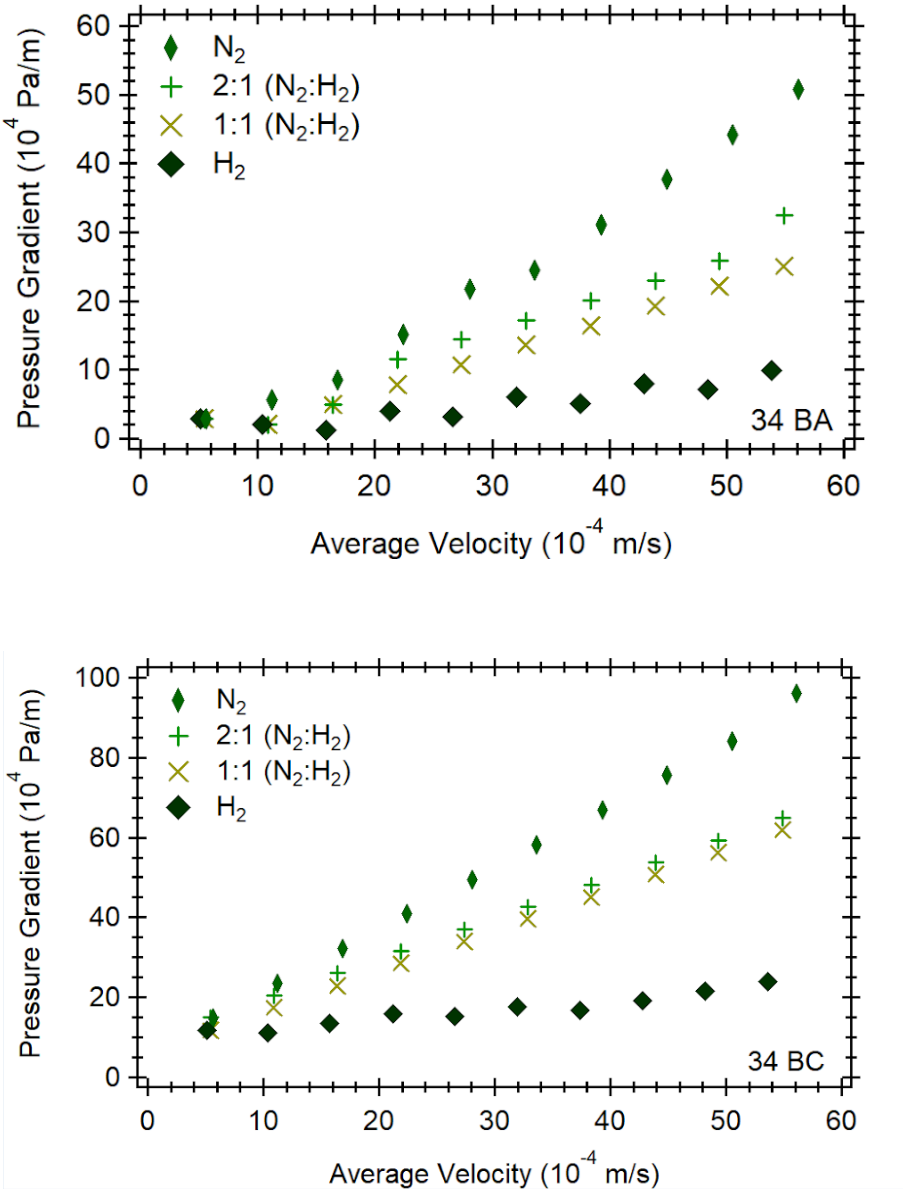

Figure 16. Pressure gradient vs average velocity for global permeability. Results are shown for 24 BA, 24 BC. 34 BA, and 34 BC. Flow rate: 50-500 NmL·min^{-1}.
Effective surface area: 1.61×10^{-3} m^2.

It was observed when using pure hydrogen that there was approximately a 16% loss in flow rates between the inlet regulated by the mass flow controller and the outlet measured by the gas flow calibrator. This is due to hydrogen's low viscosity and small size which makes it easier for the gas to escape through small leaks within the system. This is why hydrogen has a lower average velocity than the other gases. Additionally, it was observed for the various mixtures that ratios that included a larger amount of hydrogen had greater losses in gas flow when compared to ratios that did not include as much hydrogen. The ratios that included a larger amount of nitrogen were found to have higher pressure differentials than ratios that had less nitrogen. This corroborates

the findings observed when measuring the pure gases and follows the same trends associated with viscosity and molecular size.

It was expected that GDLs with an MPL present would have higher pressure gradients due to the MPL's low porosity. This was observed in for both the 24 and 34 series, where the GDL containing the MPL had a greater pressure drop across the cell than the GDL without an MPL. 24 BC was found to have the highest pressure drop, followed by 34 BC, 24 BA, and 34 BA. The 34 series had lower pressure drops than their 24 counterparts due to the lower anisotropy of the 34 series. These graphs were used to calculate permeabilities for the GDLs, which can be seen in Table 5. No literature values for global permeability were found for comparison.

Table 5. Global viscous permeability for 24 and 34 series in the multichannel cell (25 cm^2).

GDL (SGL)	Pure N_2 $m^2 \pm 10$ %	Pure H_2 $m^2 \pm 10$ %	N_2:H_2 (1:1) $m^2 \pm 10$ %	N_2:H_2 (2:1) $m^2 \pm 10$ %
24 BA	2.07×10^{-13}	2.93×10^{-13}	2.51×10^{-13}	2.18×10^{-13}
24 BC	8.44×10^{-14}	1.07×10^{-13}	1.00×10^{-13}	8.80×10^{-14}
34 BA	3.90×10^{-13}	7.42×10^{-13}	6.64×10^{-13}	6.52×10^{-13}
34 BC	9.99×10^{-14}	1.69×10^{-13}	1.36×10^{-13}	1.33×10^{-13}

Across all gas configurations, 34 BA was the most permeable, followed by 24 BA, 34 BC, and 24 BC which had the lowest permeability. This was expected, since the GDL that showed the lowest pressure drop should also show the highest permeability. It was observed that BC grades had lower permeabilities due to the presence of an MPL while GDLs that were only composed of an MPS (BA grades) had higher permeabilities. This shows how the presence of an MPL reduces porosity of the GDL and makes it more difficult for gas to flow through the layer, thus decreasing the permeability and increasing the pressure drop. Following the trends from the pressure drop graphs, the 34 series GDLs had higher permeabilities than their 24 series counterparts, due to the lower pressure drops associated with the 34 series.

The permeability values for the remaining GDLs are reported in Table 6.

Table 6. Global viscous permeability for remaining GDLs in the multichannel cell (25 cm^2).

GDL (SGL)	Pure N_2 $m^2 \pm 10$ %	Pure H_2 $m^2 \pm 10$ %	N_2:H_2 (1:1) $m^2 \pm 10$ %	N_2:H_2 (2:1) $m^2 \pm 10$ %
10 BC	9.94×10^{-14}	2.10×10^{-13}	2.02×10^{-13}	1.01×10^{-13}
24 AA	2.76×10^{-13}	5.15×10^{-13}	4.23×10^{-13}	2.77×10^{-13}
28 AA	1.84×10^{-13}	2.60×10^{-13}	2.31×10^{-13}	1.91×10^{-13}
28 BC	1.17×10^{-13}	1.55×10^{-13}	1.40×10^{-13}	1.27×10^{-13}
30 BC	1.06×10^{-13}	2.15×10^{-13}	1.71×10^{-13}	1.23×10^{-13}
38 BC	1.02×10^{-13}	1.98×10^{-13}	1.90×10^{-13}	1.67×10^{-13}

It was also observed that all GDLs had higher permeabilities when pure hydrogen was used than when pure nitrogen was used which can be attributed to the viscosity of the gas and size of the molecule. Nitrogen has a larger molecular size, so it is more difficult for the gas to diffuse across the GDL. For the ratio values of permeability, it was expected that as nitrogen content increased in the mixture, permeability would decrease due to the gas's larger size and higher viscosity. These results were expected, as the lowest permeabilities correspond to the gas with the highest pressure drop.

4.2 Fundamental Cell

4.2.1 Through-Plane Permeability

As seen in Figure 17, tests run with nitrogen yielded the largest pressure gradients, followed by mixtures 2:1 and 1:1 (N_2:H_2), and tests with hydrogen had the smallest. 24 BC produced the largest pressure gradient, followed by 34 BC, 24 BA, and 34 BA. It is important to note that the scale for the pressure gradient of 24 BC is 10^6, while the others are 10^4. 24 BC has a much larger pressure gradient than the rest of the GDLs due to its MPL. This GDL may have a high anisotropy which would correspond to less uniform fiber patterns within the MPS and result in a higher pressure drop. 34 BC has the next highest pressure gradient due to its MPL, and 24 BA follows due to its high anisotropy. 34 BA, which has no MPL and lower anisotropy, was expected to yield the lowest pressure gradient.

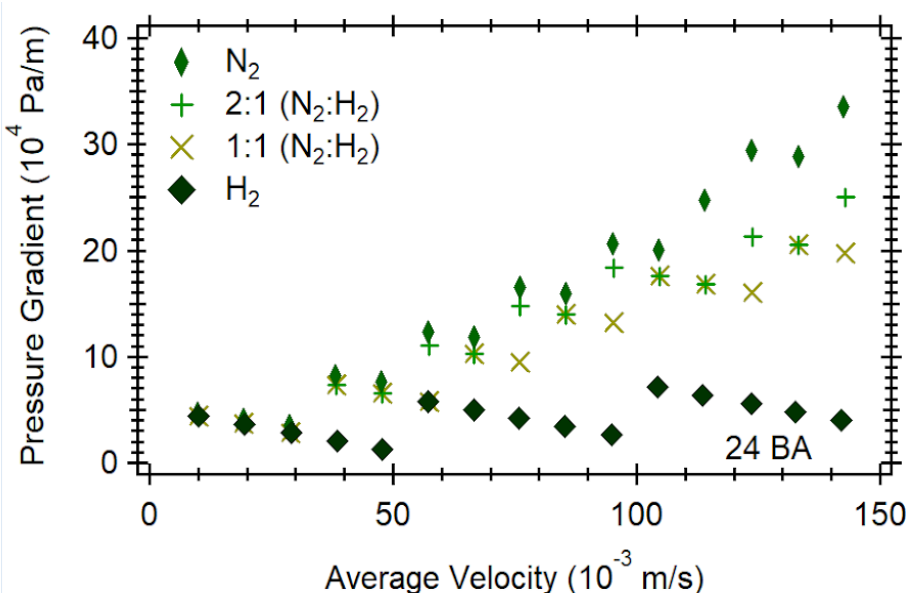
Pressure Gradient (10^4 Pa/m)
Average Velocity (10^{-3} m/s)
N_2
2:1 (N_2:H_2)
1:1 (N_2:H_2)
H_2
24 BA
0
10
20
30
40
0
50
100
150

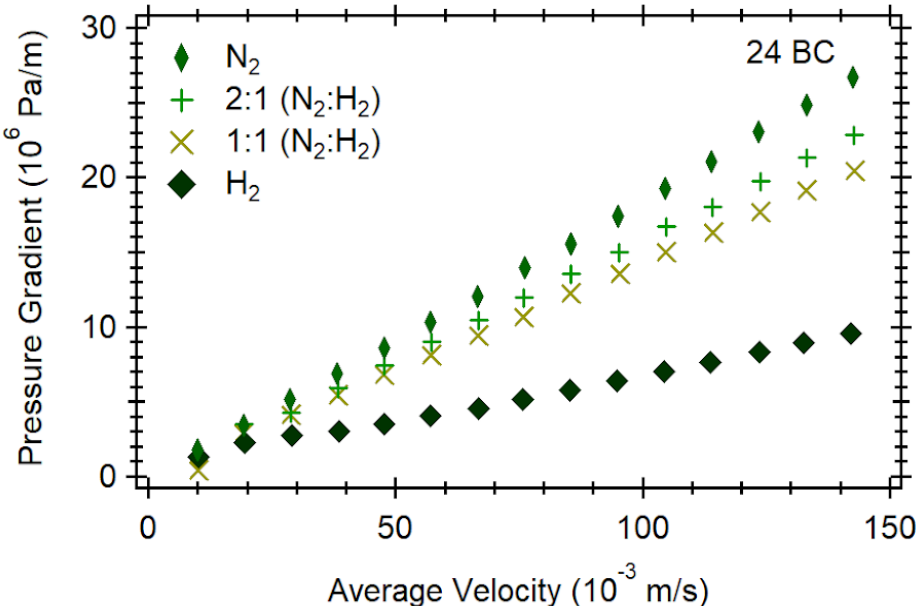
Pressure Gradient (10^6 Pa/m)
Average Velocity (10^{-3} m/s)
N_2
2:1 (N_2:H_2)
1:1 (N_2:H_2)
H_2
24 BC
0
10
20
30
0
50
100
150

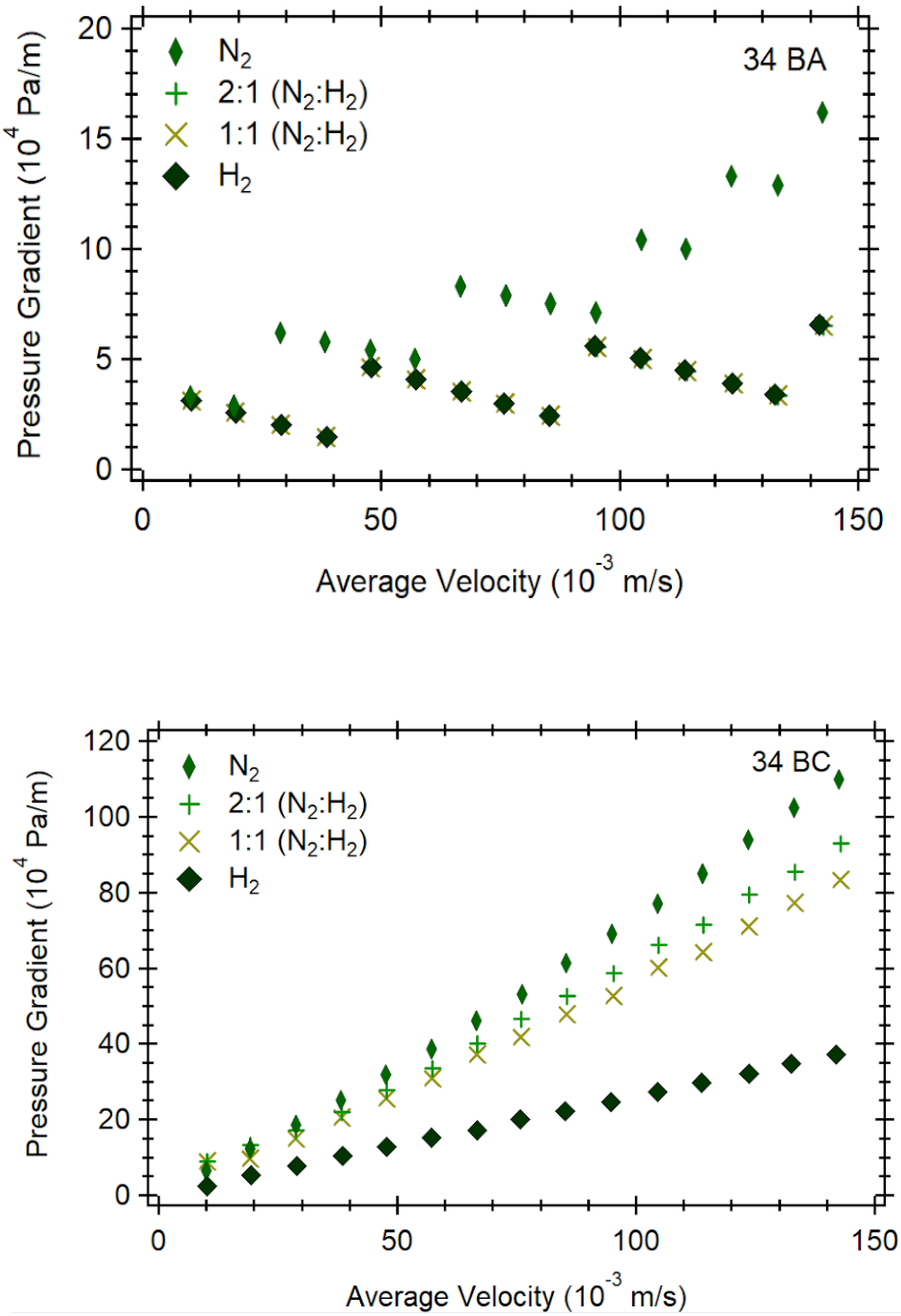

Figure 17. Pressure gradient vs average velocity for through-plane permeability. Results shown for 24 BA, 24 BC, 34 BA, and 34 BC. Flow rate: 10-150 NmL·min^{-1}. Effective surface area: 1.963 × 10^{-5} m^2.

The graphs for 24 BA and 34 BA exhibit a different, nonlinear profile, which can be explained by the differential pressure indicator displaying the same pressure drop during experimentation even though the flow rate of the gas had increased. This is due to the limited resolution and

accuracy of the differential pressure indicator as it only measures to a precision of approximately 0.1 mbar. As a result, even though the pressure was increasing as flow rate increased, the indicator was not sensitive enough to determine the pressure drop accurately. For example, 24 BA had an overall pressure drop of roughly 0.2 mbar for hydrogen in the through-plane configuration. As the precision of the differential pressure indicator is so large in comparison to the measured pressure drop, multiple flow rates read the same pressure drop value. When recording the pressure drop in the empty cell, a similar trend was seen, but a linear regression was used to fit the data in order to estimate the pressure drop at each flow rate. Therefore, when the estimated pressure drop of the empty cell was subtracted from the recorded pressure drop of the loaded cell, the pressure drop of the loaded cell appears to decrease for periods when the differential pressure indicator reading remained constant.

Using these data, the permeabilities were calculated and can be seen below in Table 7.

Table 7. Through-plane viscous permeability in the fundamental cell.

GDL (SGL)	Pure N_2 $m^2 \pm 10$ %	Pure H_2 $m^2 \pm 10$ %	N_2:H_2 (1:1) $m^2 \pm 10$ %	N_2:H_2 (2:1) $m^2 \pm 10$ %	Literature* m^2
24 BA	1.26×10^{-11}	2.01×10^{-11}	1.22×10^{-11}	9.90×10^{-12}	6.54×10^{-12} & 14.5×10^{-12} [Gostick.et.al]
24 BC	9.84×10^{-14}	1.25×10^{-13}	1.32×10^{-13}	1.04×10^{-13}	1.46×10^{-13} & 5.96×10^{-14} [Pant.et.al]
34 BA	1.45×10^{-11}	3.10×10^{-11}	2.86×10^{-11}	2.02×10^{-11}	1.88×10^{-11} [Mangal.et.al], 2.74×10^{-11} [Pant.et.al], & 1.63×10^{-11} [Gostick.et.al]
34 BC	2.81×10^{-13}	3.33×10^{-13}	2.96×10^{-13}	2.63×10^{-13}	$4.4\text{-}7.9 \times 10^{-13}$ [Pant.et.al]

*Literature values are for through-plane permeability. Each literature source developed their own cell for testing. Gases used for each source are as follows: Gostick: Air, Pant: Nitrogen, Mangal: Oxygen.

It can be seen that the values obtained experimentally are comparable to literature values and most are within the same order of magnitude. Differences in these values can be attributed to

variation in experimental procedure and equipment setup. This could lead to differences in measurement accuracy, instrumental precision, and scale of operation.

It was observed that the order of through-plane permeability was consistent across all gas configurations with 34 BA being the most permeable followed by 24 BA, 34 BC, and 24 BC which was the least permeable. Similar to global permeabilities, higher through-plane permeabilities were observed in BA grades due the higher porosity of these GDLs as compared to BC grades which have an MPL and are therefore less porous. The 24 BA GDL has a porosity of 84% and 34 BA has a porosity of 83%. In comparison, 24 BC has a porosity of only 76% and 34 BC has a porosity of only 75%. Much of the decrease in porosity can be attributed to the MPL which resulted in the BC grade GDLs having permeabilities that were 2-3 orders of magnitude smaller than the BA grades which only consist of an MPS.

4.2.2 In-Plane Permeability

As can be seen in Figure 18, the pressure gradient vs average velocity graphs for in-plane experiments show the same trend as was found for the multichannel experiments. Similarly, it was found that pure nitrogen had the highest pressure gradient followed by 2:1 (N_2:H_2), 1:1 (N_2:H_2), and pure hydrogen which can be explained by the properties of each gas. Again, it was observed that BC grade GDLs had much larger pressure gradients than the BA grade GDLs within the same series due to the presence of an MPL.

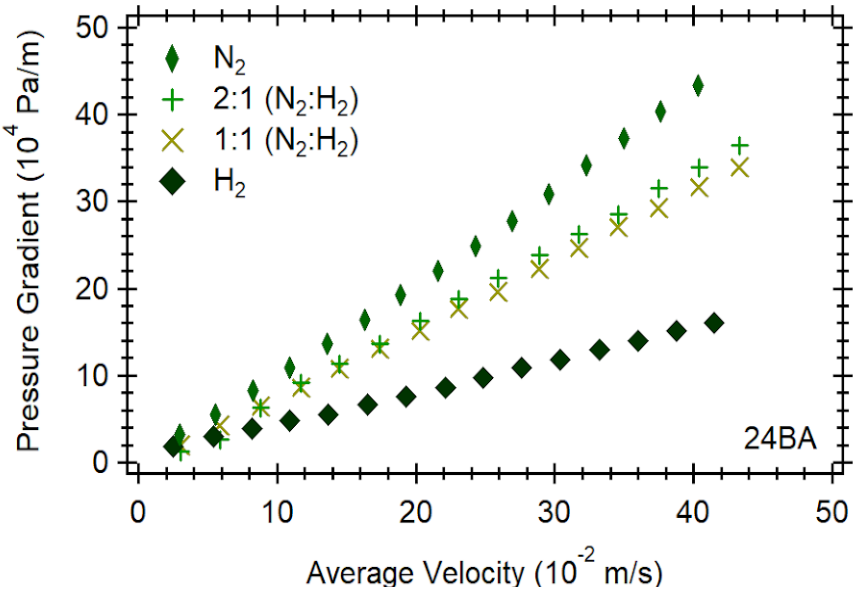

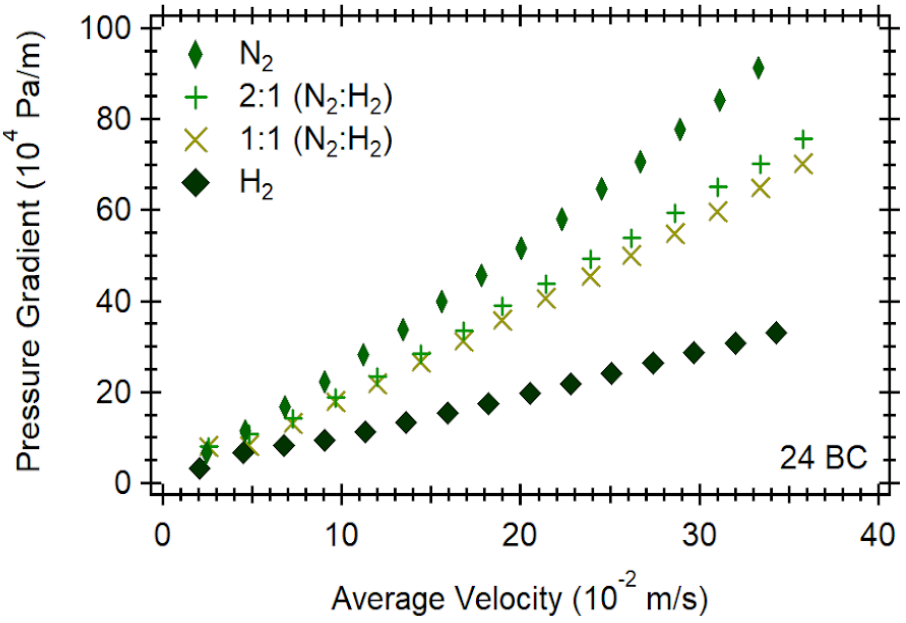
Pressure Gradient (10^4 Pa/m)
Average Velocity (10^{-2} m/s)
N_2
2:1 (N_2:H_2)
1:1 (N_2:H_2)
H_2
24 BC
0
20
40
60
80
100
0
10
20
30
40

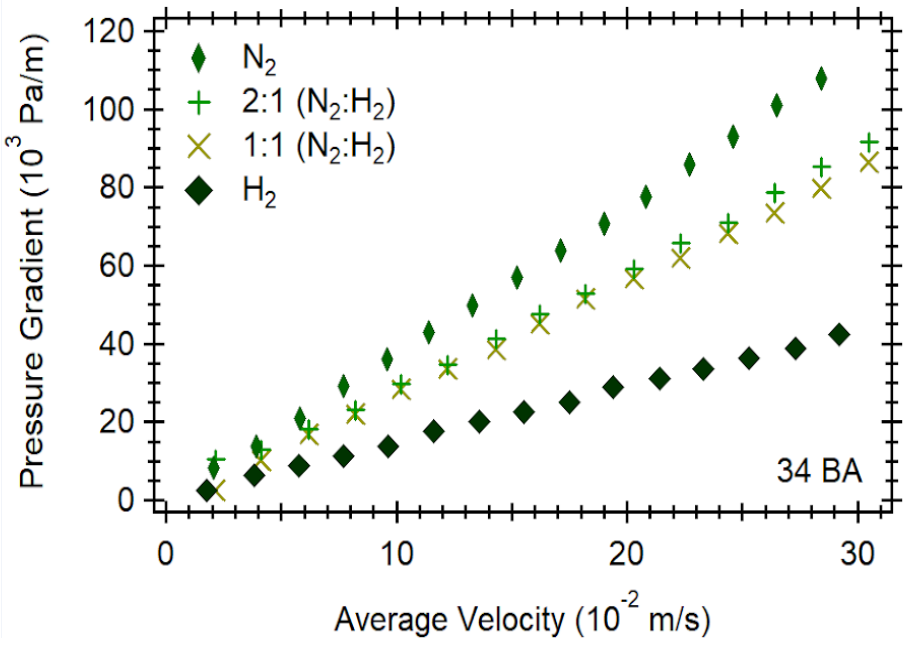
Pressure Gradient (10^3 Pa/m)
Average Velocity (10^{-2} m/s)
N_2
2:1 (N_2:H_2)
1:1 (N_2:H_2)
H_2
34 BA
0
20
40
60
80
100
120
0
10
20
30

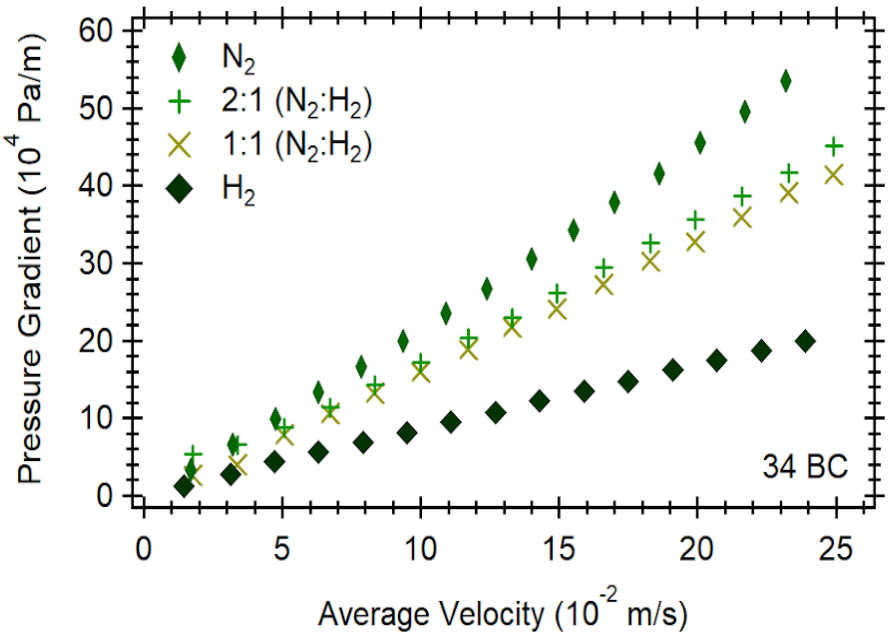

Figure 18. Pressure gradient vs average velocity for in-plane permeability. Results shown for 24 BA, 24 BC, 34 BA, and 34 BC. Flow rates: 10-150 NmL·min^{-1}. Integration of the radius used in calculations for average velocity.

It is worth noting that 34 BA has a pressure gradient that is less than all the other GDL's pressure gradients by a factor of 4-8. This corresponds to a high permeability as can be seen below in Table 8.

Table 8. In-plane viscous permeability in the fundamental cell

GDL (SGL)	Pure N_2 $m^2 \pm 10$ %	Pure H_2 $m^2 \pm 10$ %	N_2:H_2 (1:1) $m^2 \pm 10$ %	N_2:H_2 (2:1) $m^2 \pm 10$ %
24 BA	1.67×10^{-11}	2.23×10^{-11}	2.01×10^{-11}	2.05×10^{-11}
24 BC	6.65×10^{-12}	8.93×10^{-12}	8.21×10^{-12}	7.95×10^{-12}
34 BA	4.64×10^{-11}	6.02×10^{-11}	5.70×10^{-11}	5.57×10^{-11}
34 BC	7.89×10^{-12}	1.03×10^{-11}	9.62×10^{-12}	9.24×10^{-12}

Similar to through-plane permeability, for all in-plane gas configurations 34 BA was the most permeable, followed by 24 BA, 34 BC, and 24 BC which had the lowest permeability. Again, the higher permeabilities of the BA grades is due to the absence of an MPL and higher porosities.

For the 24 series, the BA permeabilities are greater by a factor of 2.5, while for the 34 series the permeabilities are greater by a factor of 6. This is due to a large fraction of the gas passing radially through the substrate region of the GDL as opposed to flowing across the MPL. Therefore, the presence of an MPL does not affect in-plane permeability as much as through-plane permeability due to the direction of gas flow.

It is also worth noting that the anisotropy of each of the GDLs impacts in-plane permeability as discussed previously for through-plane permeability. However, anisotropy has a much larger impact on in-plane permeability because gas needs to flow longer in in-plane configurations in order to travel the radius of the GDL whereas through-plane configurations require the gas to only travel a distance equivalent to the thickness of the GDL. This is exemplified by the in-plane permeability values of 24 BA and 34 BA which were 1.67×10^{-11} m^2 and 4.64×10^{-11} m^2, respectively. These values differ by 2.97×10^{-11} m^2, a percentage difference of 94.14%. The values for through-plane permeability for the same two GDLs are much closer in value with a difference of only 4.50×10^{-12} m^2 which gives a percentage difference of only 30.30%. Additional differences in values can be attributed to PTFE content and presence of an MPL.

It should be observed that there was no significant literature reporting in-plane permeability measurements, so no valid comparisons to other values could be made.

4.3 Scanning Electron Microscopy (SEM)

SEM images allow the difference in permeability to be visually understood. In Figure 19, the difference between the surface of a GDL with and without an MPL can be seen. Figure 19.A shows the carbon fibers of the MPS of 24 BA. 24 BC is coated with an MPL, which is seen in Figure 19.B.

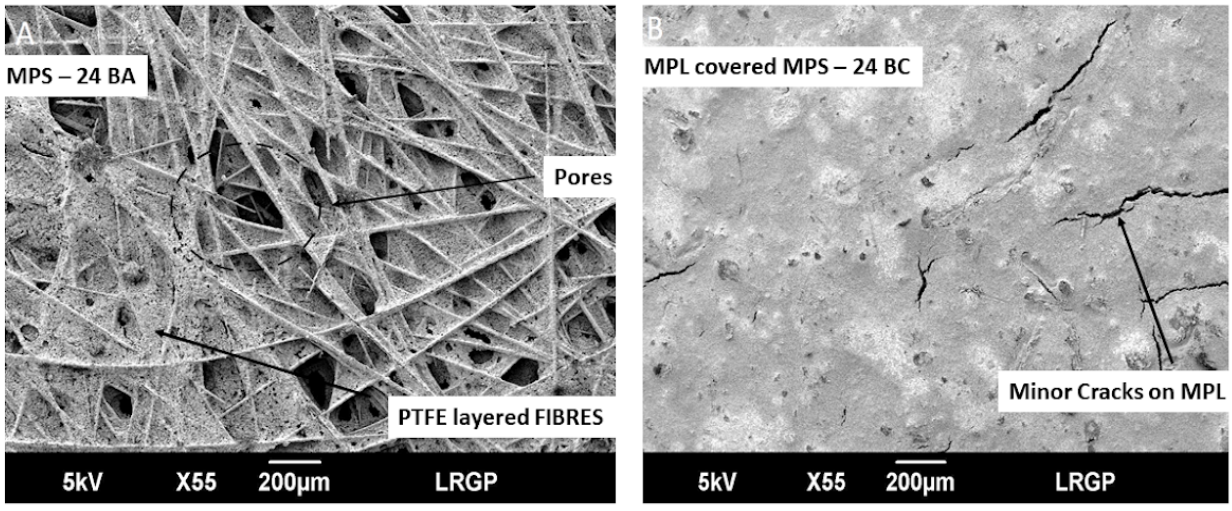

Figure 19. SEM surface images of A) 24 BA and B) the MPL layer of 24 BC.

The surface image of 24 BA shows the anisotropy of the GDL. Below the MPL of 24 BC is an MPS similar to that of 24 BA. The MPL is a relatively thin layer and therefore is very fragile, which can be seen by the formation of cracks on an unused GDL. Cracking of the MPL before use may lead to the GDL degrading more quickly. The addition of the MPL leads to a decrease in permeability. Cross-sectional images show the impregnation of the MPL on the MPS, as seen in Figure 20.

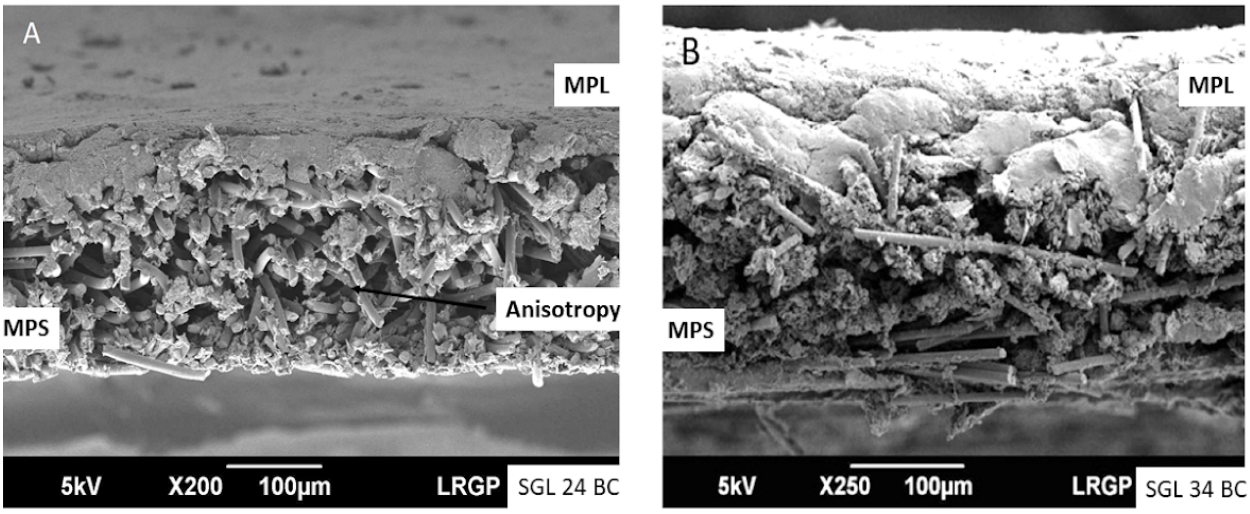

Figure 20. SEM cross-sectional images of A) 24 BC and B) 34 BC.

These cross-sectional images show the smooth top layer of the MPL with the carbon fibers of the MPS underneath. The intermediate layer that has formed between the MPS and MPL during thermal annealing can also be seen.

5. Conclusions and Recommendations

After studying GDLs with different properties, it is evident that the composition and structure of a GDL has a large impact on its permeability. It was found that a high pressure gradient across the GDL corresponded to a low permeability. In all cases, nitrogen showed the highest pressure gradient, followed by the 2:1 ratio and 1:1 ratio, with hydrogen showing the lowest pressure gradient. It was also observed that hydrogen had the highest permeability followed by the 1:1 ratio, the 2:1 ratio, and nitrogen across all gas configurations.

The main factors studied in this paper were GDL thickness and coating. While it was expected that thicker GDLs would have a lower permeability, the reverse trend was found. It is possible that this is due to the thinner GDLs (24 series) having higher anisotropy than the thicker ones (34 series). In all cases, GDLs coated with an MPL have lower permeabilities than their non-coated counterparts. However, the presence of an MPL had a greater impact on through-plane permeability than on in-plane permeability. This is due to the difference in gas flow direction which enables a majority of gas to bypass the MPL when traveling radially through the substrate layer of the GDL during in-plane testing.

References

1. A. L. Dicks, D. A. J. Rand, Fuel cell systems explained, 3rd edn., Wiley, Hoboken, 2018.
2. Proton-exchange membrane fuel cells. Wikipedia. 2019. https://en.wikipedia.org/wiki/Proton-exchange_membrane_fuel_cell
3. L.M. Pant, S.K. Mitra, M. Secanell, Absolute permeability and Knudsen diffusivity measurements in PEMFC gas diffusion layers and micro porous layers, J. Power Sources. 206 (2012) 153–160.
4. P. Mangal, L. M. Pant, N. Carrigy, M. Dumontier, V. Zingan, S. Mitra, M. Secanell, Experimental study of mass transport in PEMFCs: Through-plane permeability and molecular diffusivity in GDLs, Electrochim. Acta. 167 (2015) 160–171.
5. L. Cindrella, A.M. Kannan, J.F. Lin, K. Saminathan, Y. Ho, C.W. Lin, J. Wertz, Gas diffusion layer for proton exchange membrane fuel cells-A review, J. Power Sources. 194 (2009) 146–160.
6. F. Lapicque, M. Belhadj, C. Bonnet, J. Pauchet, Y. Thomas, A critical review on gas diffusion micro and macroporous layers degradations for improved membrane fuel cell durability, J. Power Sources. 336 (2016) 40–53.
7. X. Yu, S. Ye, Recent advances in activity and durability enhancement of Pt/C catalytic cathode in PEMFC Part II: Degradation mechanism and durability enhancement of carbon supported platinum catalyst. J. Power Sources. 172 (2007) 145-154.
8. J. Chen, T. Matsuura, M. Hori, Novel gas diffusion layer with water management function for PEMFC. J. Power Sources. 131 (2004) 155-161.
9. H. Liu, T. Zhou, Transport phenomena analysis in proton exchange membrane fuel cells, J. Heat Transfer. 127 (2005) 1363-1379.
10. End plates. Fuel Cell Store. 2019. https://www.fuelcellstore.com/fuel-cell-components/plates/end-plates
11. Information. FCSys. 2019. https://build.openmodelica.org/Documentation/FCSys.html
12. 2 typical polarization curve of a PEM fuel cell. Research Gate. 2016. https://www.researchgate.net/figure/Typical-polarization-curve-of-a-PEM-fuel-cell_fig2_314087767
13. Gas diffusion layers. Fuel Cells Etc. 2019. https://www.fuelcellsetc.com/store/Gas-Diffusion/Layers
14. H. Li, Y. Tang, Z. Wang, Z. Shi, S. Wu, D. Song, J. Zhang, K. Fatih, J. Zhang, H. Wang, Z. Liu, R. Abouatallah, A. Mazza, A review of water flooding issues in the proton exchange membrane fuel cell. J. Power Sources. 178 (2008) 103-117.
15. S. Park, J. Lee, B. N. Popov, A review of gas diffusion layer in PEM fuel cells: Materials and designs. Int. J. Hydrogen Energy. 37 (2012) 5850-5865.
16. What is the difference between carbon paper and carbon cloth based gas diffusion layers (GDL)? Fuel Cell Etc. 2019. https://fuelcellsetc.com/2013/03/comparing-gas-diffusion-layers-gdl/
17. The Editors of Encyclopaedia Britannica. Polytetrafluoroethylene. Encyclopedia Britannica. 2019. https://www.britannica.com/science/polytetrafluoroethylene

18. R. B. Ferreira, D. S. Falcão, V. B. Oliveira, A. M. F. R. Pinto, Experimental study on the membrane electrode assembly of a proton exchange membrane fuel cell: effects of microporous layer, membrane thickness and gas diffusion layer hydrophobic treatment. Electrochim. Acta. 224 (2017) 337-345.
19. J.T. Gostick, M.W. Fowler, M.D. Pritzker, M.A. Ioannidis, L.M. Behra, In-plane and through-plane gas permeability of carbon fiber electrode backing layers, J. Power Sources. 162 (2006) 228–238.
20. J.P. Feser, A.K. Prasad, S.G. Advani, Experimental characterization of in-plane permeability of gas diffusion layers, J. Power Sources. 162 (2006) 1226–1231.
21. Moldflow Flex: Preform surface- Porosity and permeability. Autodesk. 2015. https://knowledge.autodesk.com/support/moldflow-flex/learn-explore/caas/CloudHelp/cloudhelp/2016/ENU/MoldflowInsight360/files/GUID-AE4BF3C5-6650-4CF8-97E8-E5480A4A6733-htm.html
22. Navier-Stokes equation. Continuum Mechanics. 2012. http://www.continuummechanics.org/navierstokes.html
23. M.S. Ismail, D. Borman, T. Damjanovic, D.B Ingham, M. Pourkashanian, On the through-plane permeability of microporous layer-coated gas diffusion layers used in proton exchange membrane fuel cells Int.J. Hydrogen Energy 36 (2011) 10392-10402
24. D. Song, Q. Wang, Z. Liu, T. Navessin, M. Eikerling. S. Holdcroft, Numerical optimization study of the catalyst layer of PEM fuel cell cathode. J. Power Sources. 126 (2004) 104-111
25. O. M. Orogbemi, D.B. Ingham, M. S. Ismail, K. J. Hughes, L. Ma, M. Pourkashanian, The effects of the composition of microporous layers on the permeability of gas diffusion layers used in polymer electrolyte fuel cells. Int. J. Hydrogen Energy. 41 (2016) 21345-21351
26. J. Ihonen, M. Mikkola, G. Lindbergh, Flooding of gas diffusion backing in PEFCs: physical and electrochemical characterization. J. Electrochem. Soc. 151 (2004) 1152–1161.
27. Gas Diffusion Layer Comparison Chart. Fuel Cells Etc. 2019. https://fuelcellsetc.com/helpful-tools/gas-diffusion-layer-gdl-comparison-chart/
28. Sigracet. Fuel Cell Store. 2019. https://www.fuelcellstore.com/fuel-cell-components/gas-diffusion-layers/carbon-paper/sigracet
29. M. Mukherjee, C. Bonnet, F. Lapicque, A. V. Shirsath, D. Arora, S. Rael, Comparison of through-plane and in-plane gas permeability in the gas diffusion layers (GDLs) with pure and mixed dry gases, in: 8th International Conference on Fundamentals and Development of Fuel Cells, Nantes, France, 2019.